Nanophotonic switch using ZnO nanorod double-quantum-well structures

Takashi Yatsui[a)]
SORST, Japan Science and Technology Agency, Bunkyo-ku, Tokyo 113-8656, Japan

Suguru Sangu
Advanced Technology R&D Center, Ricoh Co. Ltd., Yokohama, Kanagawa 224-0035, Japan

Tadashi Kawazoe and Motoichi Ohtsu[b)]
School of Engineering, The University of Tokyo, Bunkyo-ku, Tokyo 113-8656, Japan

Sung Jin An, Jinkyoung Yoo, and Gyu-Chul Yi
National CRI Center for Semiconductor Nanorods, Pohang University of Science and Technology (POSTECH), San 31 Hyoja-dong, Pohang, Gyeongbuk 790-784, Korea and Department of Materials Science and Engineering, Pohang University of Science and Technology (POSTECH), San 31 Hyoja-dong, Pohang, Gyeongbuk 790-784, Korea

(Received 12 March 2007; accepted 5 May 2007; published online 30 May 2007)

The authors report on time-resolved near-field spectroscopy of ZnO/ZnMgO nanorod double-quantum-well structures (DQWs) for a nanometer-scale photonic device. They observed nutation of the population between the resonantly coupled exciton states of DQWs. Furthermore, they demonstrated switching dynamics by controlling the exciton excitation in the dipole-inactive state via an optical near field. The results of time-resolved near-field spectroscopy of isolated DQWs described here are a promising step toward designing a nanometer-scale photonic switch and related devices. © *2007 American Institute of Physics*. [DOI: 10.1063/1.2743949]

Systems of optically coupled quantum dots (QDs) should be applicable to quantum information processing.[1,2] Additional functional devices (i.e., nanophotonic devices[3–6]) can be realized by controlling the exciton excitation in QDs. ZnO is a promising material for room-temperature operation, owing to its large exciton binding energy[7–9] and recent achievements in the fabrication of nanorod heterostructures.[10,11] This study used time-resolved near-field spectroscopy to demonstrate the switching dynamics that result from controlling the optical near-field energy transfer in ZnO nanorod double-quantum-well structures (DQWs). We observed nutation of the population between the resonantly coupled exciton states of DQWs, where the coupling strength of the near-field interaction decreased exponentially as the separation increased.

To evaluate the energy transfer, three samples were prepared [Fig. 1(a)]: (1) single-quantum-well structures (SQWs) with a well-layer thickness of L_w=2.0 nm (SQWs), (2) DQWs with L_w=3.5 nm with 6 nm separation (1-DQWs), and (3) three pairs of DQWs with L_w=2.0 nm with different separations (3, 6, and 10 nm), where each DQW was separated by 30 nm (3-DQWs). These thicknesses were determined by the transmission electron microscopy (TEM) measurement. ZnO/ZnMgO quantum-well structures (QWs) were fabricated on the ends of ZnO nanorods with a mean diameter of 80 nm using catalyst-free metal organic vapor phase epitaxy.[10] The average concentration of Mg in the ZnMgO layers used in this study was determined to be 20 at. %.

The far-field photoluminescence (PL) spectra were obtained using a He–Cd laser (λ=325 nm) before detection using near-field spectroscopy. The near-field photoluminescence (NFPL) spectra were obtained using a He–Cd laser (λ=325 nm), collected with a fiber probe with an aperture diameter of 30 nm, and detected using a cooled charge-coupled device through a monochromator. Blueshifted PL peaks were observed at 3.499(I_S), 3.429(I_{1D}), and 3.467 (I_{3D}) eV in the far- and near-field PL spectra [Fig. 2(a)]. We believe that these peaks originated from the respective ZnO QWs because their energies are comparable to the predicted ZnO well-layer thicknesses of 1.7(I_S), 3.4(I_{1D}), and 2.2 (I_{3D}) nm, respectively, calculated using the finite square-well potential of the quantum confinement effect in ZnO SQWs.[10] To confirm the near-field energy transfer between QWs, we compared the time-resolved near-field PL (TR_{NFPL}) signals at the I_S, I_{1D}, and I_{3D} peaks. For the time-resolved near-field spectroscopy, the signal was collected with a fiber probe with an aperture diameter of 30 nm and detected using a microchannel plate through a bandpass filter with 1 nm spectral width. Figure 2(b) shows the typical TR_{NFPL} of SQWs (TR_S), 1-DQWs (TR_{1D}), and 3-DQWs (TR_{3D}), respectively, using the 4.025 eV (λ=308 nm) light with a pulse of 10 ps duration to excite the barrier layers of ZnO QWs.

We calculate the exciton dynamics using quantum mechanical density-matrix formalism,[12,13]

$$\dot{\rho} = -\frac{i}{\hbar}[H,\rho] + \sum_n \frac{\gamma_n}{2}(2A_n\rho A_n^\dagger - A_n^\dagger A_n\rho - \rho A_n^\dagger A_n) \qquad (1)$$

(ρ: density operator, H: Hamiltonian in the considered system, $A_n^\dagger$ and A_n: creation and annihilation operators for an exciton energy level labeled n, and γ_n: photon or phonon relaxation constant). The exciton population is calculated using matrix elements for all exciton states in the system considered. First, we apply the calculation to a three-level system of SQWs [inset of Fig. 2(c)], where the continuum state $\hbar\Omega_C$ is initially excited using a 10 ps laser pulse. Then, the initial exciton population in ZnO QWs is created in $\hbar\Omega_{1S}$, where an incoherent Gaussian excitation term with a tempo-

a)Electronic mail: yatsui@ohtsu.jst.go.jp
b)Also at SORST, Japan Science and Technology Agency, 2-11-16 Yayoi, Bunkyo-ku, Tokyo 113-8656, Japan.

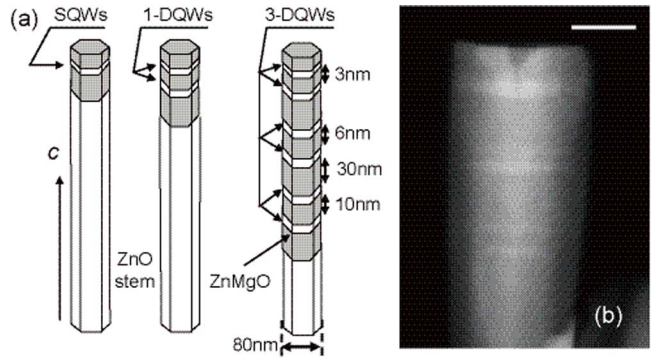

FIG. 1. ZnO/ZnMgO nanorod quantum-well structures. c: *c* axis of the ZnO stem. (a) Schematics of ZnO/ZnMgO SQWs, DQWs (1-DQWs), and triple pairs of DQWs (3-DQWs). (b) *Z*-contrast TEM image of 3-DQWs clearly shows the compositional variation, with the bright layers representing the ZnO well layers. Scale bar: 50 nm.

ral width of $2\sigma_{1S}$ is added in Eq. (1) because nonradiative relaxation paths via exciton-phonon coupling make a dephased input signal, statistically. Finally, an exciton carrier relaxes due to the electron-hole recombination with relaxation constant γ_{1S}. Figure 2(c) shows a numerical result and experimental data. Here, we used $2\sigma_{1S}=100$ ps, and γ_{1S} was evaluated as 460 ps.

A similar calculation was applied for DQWs. We used two three-level systems, coupled via an optical near field with a coupling strength of U_{12} [inset of Fig. 2(d)]. Figure 2(d) shows the numerical results for the exciton population in QWs_1 and the experimental data. Here $2\sigma_{1D}$ and $2\sigma_{2D}$ were set at 200 ps, which is twice the value for SQWs, because the relaxation paths extend the barrier energy state in the two quantum well (QW). γ_{1D} and γ_{2D} are evaluated as 200 ps. We believe that the faster relaxation for DQWs compared with SQWs reflects the lifetime of the coupled states mediated by the optical near-field. Furthermore, the characteristic behavior that results from near-field coupling appears as the oscillatory decay in Fig. 2(d). This indicates that the time scale of the near-field coupling is shorter than the decoherence time, and that coherent coupled states, such as symmetric and antisymmetric states,[14] determine the system dynamics. Furthermore, nutation never appears unless unbalanced initial exciton populations are prepared for $\hbar\Omega_{1D}$ and $\hbar\Omega_{2D}$. In the far-field excitation, only the symmetric state is excited because the antisymmetric state is dipole inactive. By contrast, in the near-field excitation, both the symmetric and antisymmetric states are excited due to the presence of a near-field probe. Since the symmetric and antisymmetric states have different eigenenergies, the interference of these states generates a detectable beat signal. The unbalanced excitation rate is given by $A_1/A_2=10$ here. From the period of nutation, the strength of the near-field coupling is estimated to be $U_{12}=7.7$ ns^{-1} (=4.9 μeV).

We evaluated nutation frequencies using Fourier analysis. In Fig. 3(a), the power spectral density of SQWs (PS_S) does not exhibit any peaks, indicating a monotonic decrease. By contrast, the power spectral density of 1-DQWs (PS_{1D}) had a strong peak at a frequency of 2.6 ns^{-1}. Furthermore, that of 3-DQWs (PS_{3D}) had three peaks at 1.9, 4.7, and 7.1 ns^{-1}. Since, the degree of the coupling strength, which is proportional to the frequency of the nutation, increases as the separation decreases, the three peaks correspond to the signals from DQWs with separations of 10, 6, and 3 nm, respectively. Since the coupling strength $\hbar U$ (eV) is given by $\hbar\pi f$ (f: nutation frequency), $\hbar U$ are estimated as 4.0, 9.9, and 14.2 μeV for DQWs with respective separations of 10, 6, and 3 nm. Furthermore, the peak intensity for the DQWs with 3 nm separation is much lower than for those with 10 nm separation, which might be caused by decoherence of the exciton state due to penetration of the electronic carrier. Considering the carrier penetration depth, the strong peak of DQWs with 10 nm separation originates from the near-field coupling alone. The solid line in Fig. 3(b) shows the separation dependence of the peak frequency. The exponentially

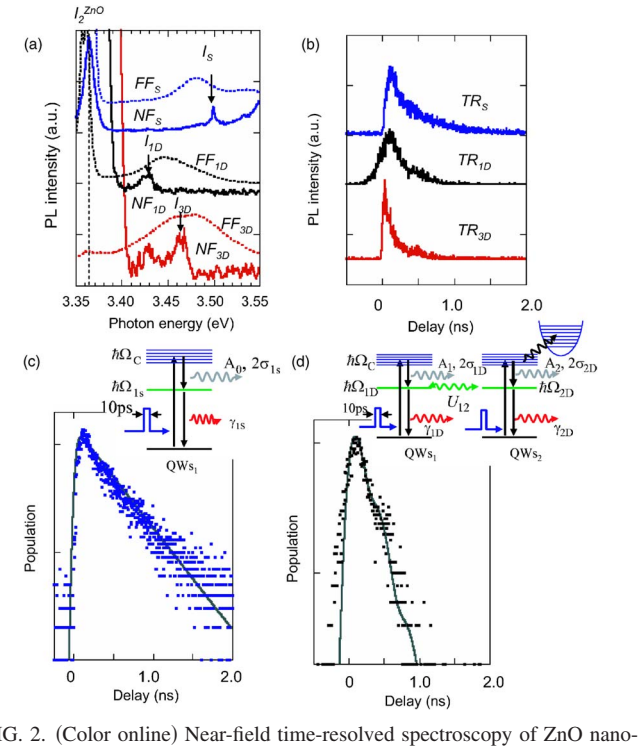

FIG. 2. (Color online) Near-field time-resolved spectroscopy of ZnO nanorod DQWs at 15 K. (a) NF_S, NF_{1D}, and NF_{3D}: near-field PL spectra. FF_S, FF_{1D}, and FF_{3D}: far-field PL spectra of ZnO SQWs (Lw=2.0 nm), 1-DQWs (Lw=3.5 nm, 6 nm separation), and 3-DQWs (Lw=2.0 nm and 3, 6, and 10 nm separation). (b) TR_S, TR_{1D}, and TR_{3D} show TR_{NFPL} signal obtained at I_S, I_{1D}, and I_{3D}. Theoretical results on the transient exciton population dynamics (solid curves) and experimental PL data (filled squares) of (c) SQWs [same as curve TR_S in (b)] and (d) 1-DQWs [same as curve TR_{1D} in (b)]. The insets schematically depict the respective system configurations. $\hbar\Omega_C$: barrier energy state with a central energy.

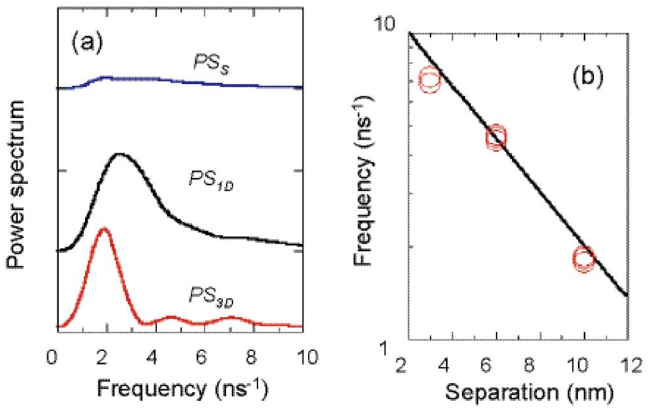

FIG. 3. (Color online) Evaluation of the nutation frequencies between the QWs. (a) PS_S, PS_{1D}, and PS_{3D} show the power spectra of TR_S, TR_{1D}, and TD_{3D}, respectively. (b) Separation D dependence of frequency of the nutation.

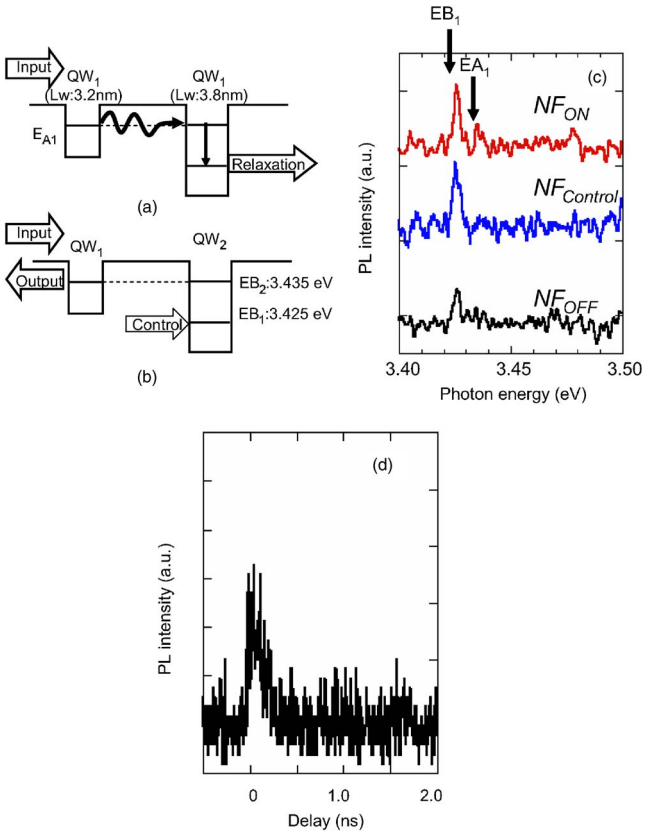

FIG. 4. (Color online) Switching operation by controlling the exciton excitation. Schematic of the nanophotonic switch of (a) "off" state and (b) "on" state. (c) NF_{on}, $NF_{control}$, and NF_{off} show NFPL signal obtained with the illumination of input laser along, control laser alone, and input and control laser, respectively. (d) Near-field time-resolved PL signal with on state.

decaying dependence represented by this line supports the origin of the peaks in the power spectra from the localized near-field interaction between the QWs.

Next, we performed the switching operation. Figures 4(a) and 4(b) explain the "off" and "on" states of the proposed nanophotonic switch, consisting of two coupled QWs. QW_1 and QW_2 are used as the input/output and control ports of the switch, respectively. Assuming L_w=3.2 and 3.8 nm, the ground exciton state in QW_1 and the first excited state in QW_2 resonate. In the off operation [Fig. 4(a)], all the exciton energy in QW_1 is transferred to the excited state in the neighboring QW_2 and relaxes rapidly to the ground state. Consequently, no output signals are generated from QW_1. In the on operation [Fig. 4(b)], the escape route to QW_2 is blocked by the excitation of QW_2, owing to state filling in QW_2 on applying the control signal; therefore, an output signal is generated from QW_1.

Figure 4(c) shows the NFPL for the three pairs of DQWs with L_w=3.2 and 3.8 nm with different separations (3, 6, and 10 nm). Curve NF_{off} was obtained with continuous input light illumination from a He–Cd laser (3.814 eV). No emission was observed from the exciton ground state of QW_1 (EA_1) or the excited state of QW_2 (EB_2) at a photon energy of 3.435 eV, indicating that the excited energy in QW_1 was transferred to the excited state of QW_2. Furthermore, the excited state of QW_2 is a dipole-forbidden level. Curve $NF_{control}$ shows the NFPL signal obtained with control light excitation of 3.425 eV with a 10 ps pulse. Emission from the ground state of QW_2 at a photon energy of 3.425 eV was observed. Both input and control light excitations resulted in an output signal with an emission peak at 3.435 eV, in addition to the emission peak at 3.425 eV (curve NF_{on}), which corresponds to the ground state of QW_2. Since the excited state of QW_2 is a dipole-forbidden level, the observed 3.435 eV emission indicates that the energy transfer from the ground state of QW_1 to the excited state of QW_2 was blocked by the excitation of the ground state of QW_2.

Finally, the dynamic properties of the nanophotonic switching were evaluated by using the time correlation single photon counting method. We observed TR_{NFPL} signals using a fiber probe with an aperture diameter of 30 nm at 3.435 eV with both input and control laser excitations [see Fig. 4(d)]. The decay time constant was found to be 483 ps. The output signal increased synchronously, within 100 ps, with the control pulse. Since the rise time is considered equal to one-quarter of the nutation period τ,[15] the value agrees with those obtained for DQWs with the same well width in the range from $\tau/4=36$ ps (3 nm separation) to $\tau/4=125$ ps (10 nm separation).

We observed the nutation between DQWs and demonstrated the switching dynamics by controlling the exciton excitation in the QWs. For room-temperature operation, since the spectral width reaches thermal energy (26 meV), a higher Mg concentration in the barrier layers and narrower L_w are required so that the spectral peaks of the first excited state (E_2) and ground state (E_1) do not overlap. This can be achieved by using two QWs with L_w=1.5 nm (QW_1) and 2 nm (QW_2) with a Mg concentration of 50%, where the energy difference between E_2 and E_1 in QW_2 is 50 meV.[16]

The work at POSTECH was supported by the National Creative Research Initiative Project, Korea and AOARD 04-49 (Quotation No. FA5209-040T0254).

[1]M. Bayer, P. Hawrylak, K. Hinzer, S. Fafard, M. Korkusinski, Z. R. Wasilewski, O. Stern, and A. Forchel, Science **291**, 451 (2001).
[2]E. A. Stinaff, M. Scheibner, A. S. Bracker, I. V. Ponomarev, V. L. Korenev, M. E. Ware, M. F. Doty, T. L. Reinecke, and D. Gammon, Science **311**, 636 (2002).
[3]M. Ohtsu, K. Kobayashi, T. Kawazoe, S. Sangu, and T. Yatsui, IEEE J. Sel. Top. Quantum Electron. **8**, 839 (2002).
[4]T. Kawazoe, K. Kobayashi, S. Sangu, and M. Ohtsu, Appl. Phys. Lett. **82**, 2957 (2003).
[5]T. Kawazoe, K. Kobayashi, K. Akahane, M. Naruse, N. Yamamoto, and M. Ohtsu, Appl. Phys. B: Lasers Opt. **84**, 243 (2006).
[6]M. Naruse, T. Miyazaki, F. Kubota, T. Kawazoe, K. Kobayashi, S. Sangu, and M. Ohtsu, Opt. Lett. **30**, 201 (2005).
[7]A. Ohtomo, K. Tamura, M. Kawasaki, T. Makino, Y. Segawa, Z. K. Tang, K. L. Wong, Y. Matsumoto, and H. Koinuma, Appl. Phys. Lett. **77**, 2204 (2000).
[8]M. H. Huang, S. Mao, H. Feick, H. Yan, Y. Wu, H. Kind, E. Weber, R. Russo, and P. Yang, Science **292**, 1897 (2001).
[9]H. D. Sun, T. Makino, Y. Segawa, M. Kawasaki, A. Ohtomo, K. Tamura, and H. Koinuma, J. Appl. Phys. **91**, 1993 (2002).
[10]W. I. Park, G.-C. Yi, M. Y. Kim, and S. J. Pennycook, Adv. Mater. (Weinheim, Ger.) **15**, 526 (2003).
[11]W. I. Park, S. J. An, J. Long, G.-C. Yi, S. Hong, T. Joo, and M. Y. Kim, J. Phys. Chem. B **108**, 15457 (2004).
[12]B. Coffey and R. Friedberg, Phys. Rev. A **17**, 1033 (1978).
[13]K. Kobayashi, S. Sangu, T. Kawazoe, and M. Ohtsu, J. Lumin. **112**, 117 (2005).
[14]S. Sangu, K. Kobayashi, A. Shojiguchi, and M. Ohtsu, Phys. Rev. B **69**, 115334 (2004).
[15]S. Sangu, K. Kobayashi, T. Kawazoe, A. Shojiguchi, and M. Ohtsu, Trans. Mater. Res. Soc. Jpn. **28**, 1035 (2003).
[16]W. I. Park, G.-C. Yi, and M. Jang, Appl. Phys. Lett. **79**, 2022 (2001).